JOURNAL OF MATERIALS SCIENCE 14 (1979) 49–58

The mechanical properties of $(SN)_x$ single crystals*

NORMAN BROWN
Department of Metallurgy and Materials Science and Laboratory for Research on the Structure of Matter, University of Pennsylvania, Philadelphia, Pa 19104, USA

C. K. CHIANG
Department of Physics and Laboratory for Research on the Structure of Matter, University of Pennsylvania, Philadelphia, Pa 19104, USA

The compression stress–strain behaviour of single crystals of sulphur nitride, $(SN)_x$, a metallic polymer, was measured in the ambient environment. Measurements were made both parallel and perpendicular to the chain axis on crystals which were about 1 mm in size. The plastic stress–strain behaviour resembled that of a highly anisotropic metal. Deformation to large strains produced a fibrilated structure which graphically exhibits the polymeric nature of $(SN)_x$. Young's moduli parallel and perpendicular to the chain were 21 and 1.4 GPa respectively. An analysis of the possible slip systems in $(SN)_x$ indicated that there is only one easy glide system, (1 0 0) [0 0 1].

1. Introduction

We report in this paper a first investigation on the stress–strain behaviour of $(SN)_x$. Polymeric sulphur nitride, $(SN)_x$, is the first known example of a metallic polymer [1–9]. It is of great interest to know its elastic and plastic properties. Because most polymers are insulators, the most intriguing question to ask was whether $(SN)_x$ would behave mechanically more like a metal or a polymer. We describe a series of measurements and experimental results which lead to the conclusion that the stress–strain behaviour of $(SN)_x$ most resembled that of a highly anisotropic metal.

$(SN)_x$ is metallic [1–7] in that its room temperature electrical conductivity in the chain direction is greater than 3×10^3 $(\Omega\,\mathrm{cm})^{-1}$, and by comparison that of mercury is 10.4×10^3 $(\Omega\,\mathrm{cm})^{-1}$. The conductivity at 4.2 K reaches 200 times that at 298 K and becomes superconducting below 0.3 K. Its colour is like bright gold.

$(SN)_x$ is also polymeric [8, 9]; it consists of nearly planar *cis–trans* chains with alternating atoms of sulphur and nitrogen. The S–N bond distances along the chain are 1.593 and 1.628 Å which indicates a covalent nature. The interchain S–N and S–S bond distances correspond to radii of 1.74 and 1.52 Å for S and N respectively; these values are slightly less than the van der Waals radii of 1.80 and 1.55 Å as compiled by Bondi [10]. $(SN)_x$ has a monoclinic crystal structure (space group $P2_1/c$), $a = 4.153$ Å, $b = 4.439$ Å, $c = 7.637$ Å and $\beta = 109.7°$ with four S–N units per unit cell. Two views of the crystal structure are shown for the plane that contains the plane of the chains $(\bar{1}\,0\,2)$, and for the plane perpendicular to the chains (1 1 0) (Fig. 1) [9].

$(SN)_x$ [8, 9, 11] polymerizes in the solid state from a crystal of disulphur dinitride S_2N_2 which occurs as planar square molecules. The transformation from S_2N_2 to $(SN)_x$ is illustrated in Fig. 2 [9]. Since the S_2N_2 molecules have two possible ways of opening, the $(SN)_x$ crystals contain two domains whose boundaries are parallel to the chain axis. The domains have a twinned orientation. The striations in Fig. 3 are probably from the twinned structure. The thickness of the domains range from about 10 Å upward and their length is about the length of the crystal. Details of

*Supported by the National Science Foundation MRL Program under Grant No. DMR 76-80994.

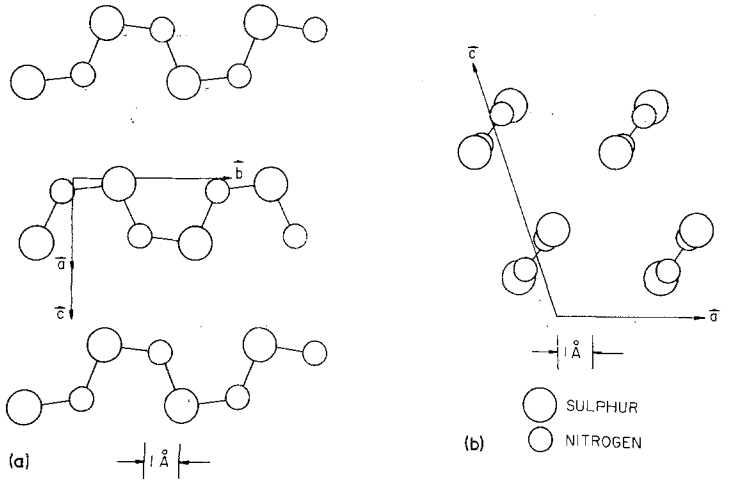

Figure 1 Crystal structure of $(SN)_x$; (a) projected onto the $(\bar{1}\,0\,2)$ plane, (b) projected onto the $(0\,1\,0)$ plane.

the size distribution of the domains are under investigation.

A full description of the preparation of S_2N_2 is given by Mikulski *et al.* [8]. S_2N_2 is made by passing S_4N_4 vapour over silver wool at 200° C and allowing the resulting S_2N_2 vapour to condense on a cold finger at 78 K. Small crystals form about 2 mm or less in size. The S_2N_2 transforms to $(SN)_x$ when it is heated to about 0° C. Six weeks at room temperature completely transforms the S_2N_2. $(SN)_x$ begins to sublime at 140 to 150° C and begins to decompose at 208° C. $(SN)_x$ is stable at room temperature and will retain its bright gold colour indefinitely in the absence of air.

Since the crystals were only about 1 mm in size, the stress–strain behaviour was measured in compression.

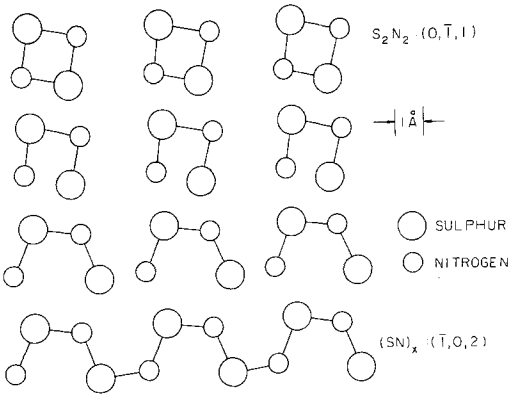

Figure 2 The polymerization of S_2N_2 to $(SN)_x$. The top view is a projection of the S_2N_2 structure onto the $(0\,\bar{1}\,0)$ plane with the *a*-axis horizontal. The bottom view is a projection of the $(SN)_x$ structure onto the $(\bar{1}\,0\,2)$ plane with the *b*-axis horizontal. The middle views show schematically the polymerization process.

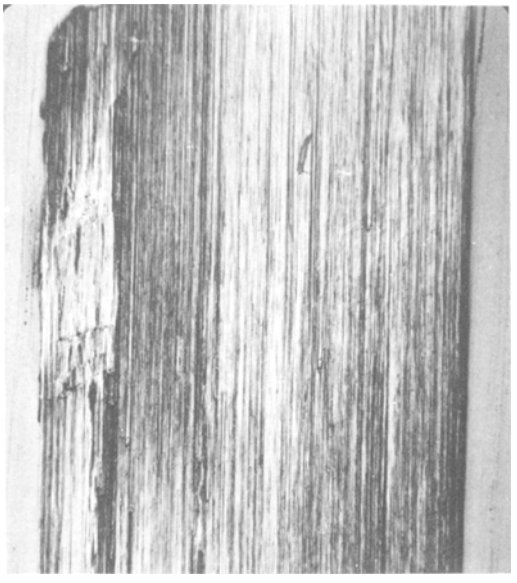

Figure 3 the surface of $(SN)_x$ single crystal under 61 times magnification. The striations are parallel to the chain direction.

Only two orientations were investigated, with the stress parallel and perpendicular to *b* (the chain axis). For the stress perpendicular to *b*, the plane of compression was not determined. The imperfect nature of the crystal surfaces and the fact that the surfaces were difficult to polish prevented the observation of slip lines and the direct determination of possible slip systems.

From an analysis of the crystal structure and the deformed crystals, we made a speculation on the slip system with lowest Peierls–Nabarro force. This speculation was supported by the observation and analysis of a stress-induced phase transformation in $(SN)_x$ by Baughman *et al.* [12–14]. At

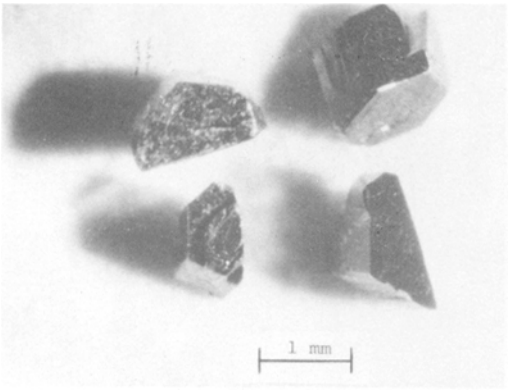

Figure 4 Typical crystals.

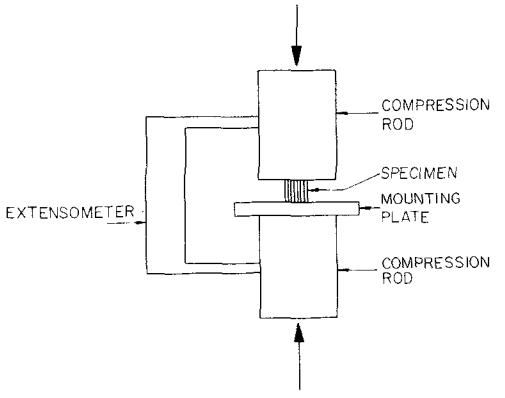

Figure 5 Schematic arrangement of mechanical testing.

this time we believe the slip system of easiest glide is (1 0 0), [0 0 1]. Large deformations produced a fibrilated structure which strongly exhibits the polymeric nature of $(SN)_x$.

2. Experimental

2.1. Materials

The $(SN)_x$ was made by the method of Mikulski *et al.* The composition is exactly stoichiometric, within the error of analysis. The material is of high purity with the combined C, O, and H being less than 0.01%. The $(SN)_x$ was free of the S_2N_2 isomer. The crystals of $(SN)_x$ were at room temperature for longer than six weeks before testing so that they were completely polymerized [9].

In a typical preparation, about 0.7 g of golden crystals of $(SN)_x$ were obtained from the original 1.20 g of S_4N_4. Only a few per cent by weight of the batch of $(SN)_x$ crystals were suitable for testing. The specimens were carefully selected from a batch on the basis of size, geometric regularity, and crystalline perfection. The crystals were the best available and were not machined or polished because methods have not been developed. They were approximately flat and parallel. The size of the crystals was about 1 mm and typical shapes of the crystal, which were tested, are shown in Fig. 4.

2.2. Test method

For testing, the crystals were glued on a 1.5 mm thick steel plate with the *b* direction parallel or perpendicular to the surface. The orientation was easily determined under a low power magnifier because the crystal surfaces parallel to *b* were brighter and flatter than the surface perpendicular to *b*. The arrangement for compressing the crystals with an Instron machine and measuring the deformation is illustrated in Fig. 5.

The crystals were photographed at 25 × magnification before and after deformation. The error in determining the cross-sectional area was about ±10% and about ±20% for the gauge length. The load was known within ±2% so that the average stress was measured to within about ±12%. The extensometer was operated at a sensitivity of about 10^{-3} mm, but since the crystals were not perfectly flat and since the crystal deformation was only a fraction of the *total* overall deformation measured within the $\frac{1}{2}$ in. span of the extensometer, the absolute value of the strain could not be obtained directly from the extensometer output. The strain axis was calibrated by two methods: (1) the strain was determined from the photographs before and after deformation and (2) the stress–strain behaviour of a small 1 mm thick specimen of polymethylmethacrylate was measured in the apparatus and compared with a precision stress–strain curve from a larger specimen. The strain rates of the test were about 10^{-1} min^{-1} and all experiments were conducted at room temperature.

Because the natural surfaces were not perfectly flat and parallel, the shape of the initial part of the stress–strain curves was largely determined by the flattening of irregularities on the specimen. After the flattening had occurred the crystals behaved in a consistent fashion and the effects of anisotropy could be observed.

3. Results

3.1. Stress–strain behaviour

The compression stress–strain behaviour of 15 crystals was observed. The initial part of all the stress–strain curves did not reflect the intrinsic

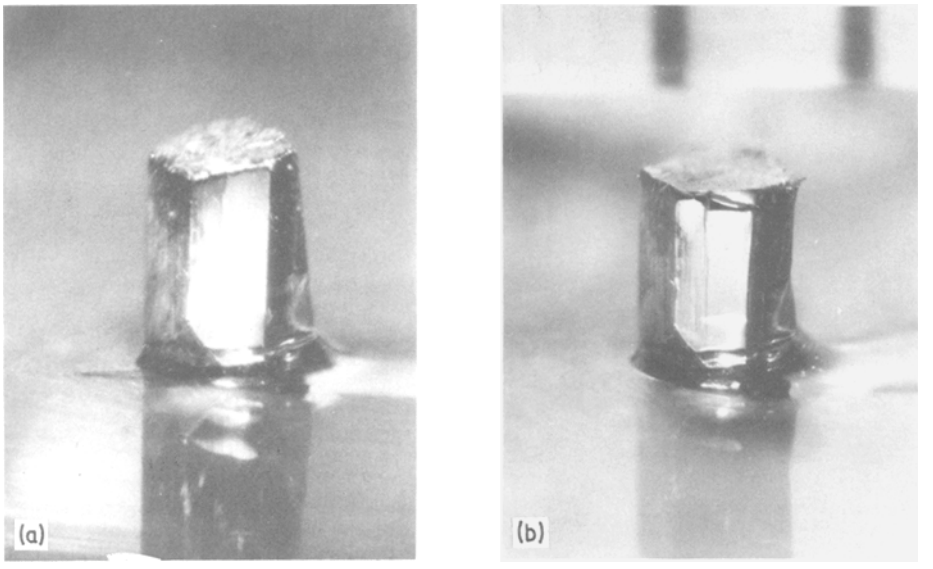

Figure 6 Photographs of crystal C; (a) before deformation, (b) after deformation.

behaviour of the material because the crystals were somewhat irregular in shape and the initially compressed surfaces were not completely flat or parallel to the compression plate. After the surface had been flattened, all crystals could be unloaded and loaded elastically and a distinct yield point could be observed upon reloading. The yield point on reloading was always about equal to the stress prior to unloading in accordance with typical metallic behaviour.

3.1.1. Stress parallel to b

Fig. 6a shows a crystal before testing and Fig. 7 is its stress–strain curve. The initial slope of the curve is not significant. After flattening the unloading–reloading behaviour is elastic, and the yield point upon reloading is about the same as the stress prior to unloading. This is typical metallic behaviour. The shape of the crystal, after the 12% strain indicated in Fig. 7, is shown in Fig. 6b. It can be seen that practically all of the observed deformation occurred by flattening the crystal. This crystal supported an average stress of 31 MPa based on its original cross-section and probably supported a true stress of about 17 MPa based on its final cross-section.

Fig. 8 shows the stress–strain curve of a crystal with stress parallel to *b* and which was deformed until the crystal collapsed as shown in Fig. 9. Again the shape of the curve before 10% strain is

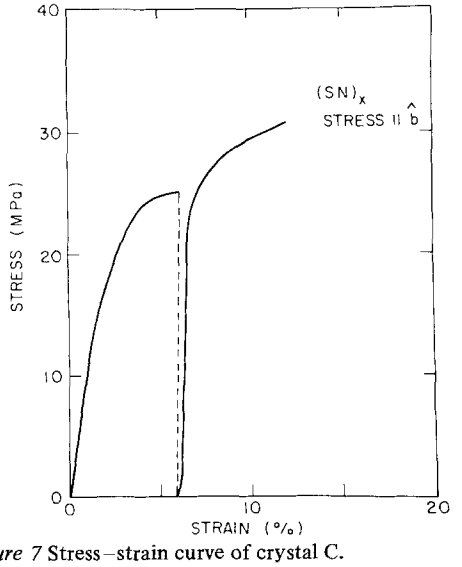

Figure 7 Stress–strain curve of crystal C.

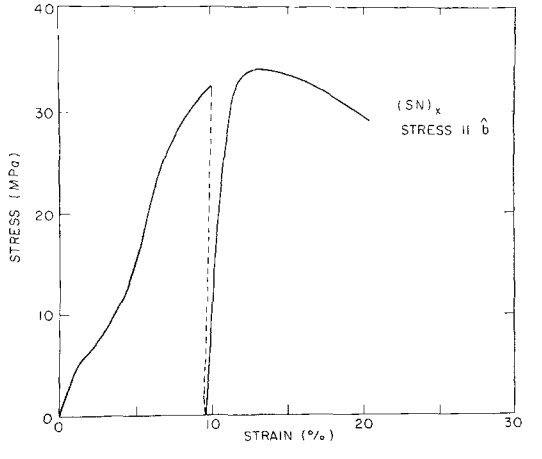

Figure 8 Stress–strain curve of crystal B.

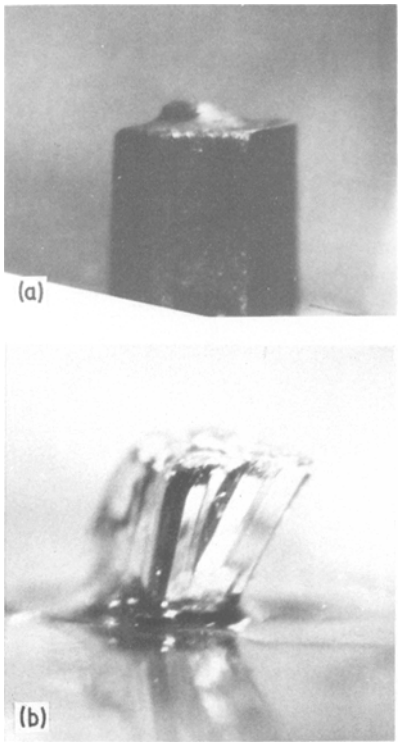

Figure 9 Photographs of crystal B; (a) before deformation, (b) after failure.

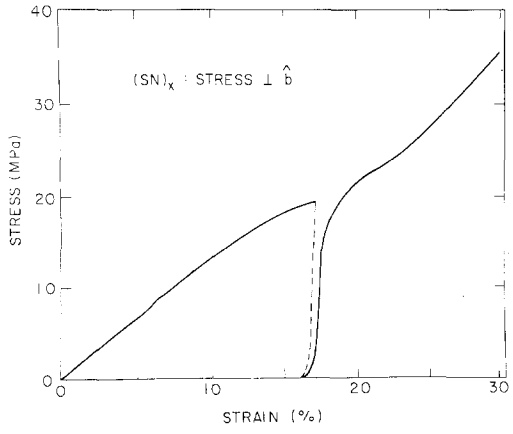

Figure 10 Stress–strain curve for crystal G.

not significant. The loading–unloading behaviour is again typically metallic. The maximum in the curve occurred when the crystal began to splinter and fibrilate. If the crystal of Fig. 6 had been compressed a little more, it probably would have also collapsed and exhibited a maximum in the stress–strain curve.

Fig. 8 is the typical behaviour for all crystals with the stress parallel to *b*. The ultimate compressive strength for these crystals ranged from 74

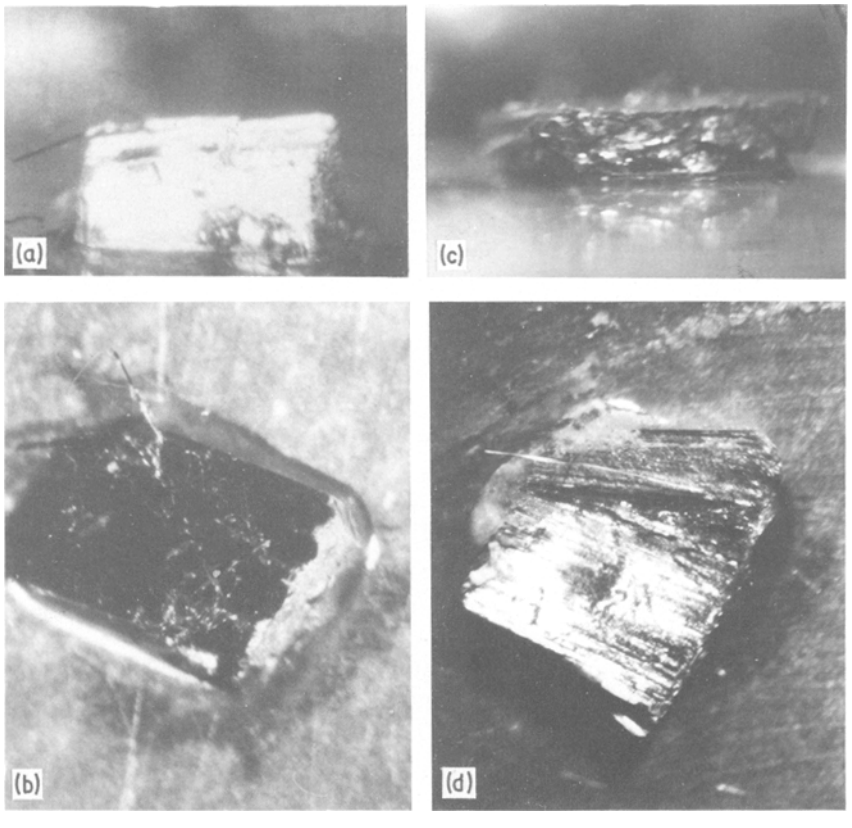

Figure 11 Photographs of crystal G: (a) side view and (b) top view before deformation; (c) side view and (d) top view after deformation.

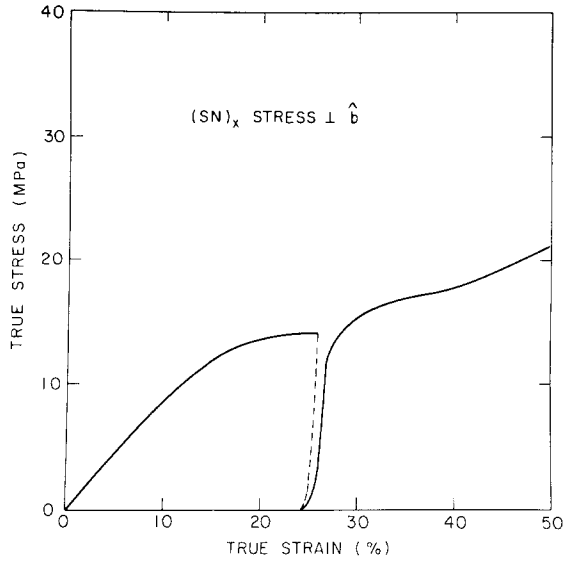

Figure 12 True stress–strain curve for crystal G.

to 15 MPa. No doubt the ultimate strength depends critically on the flatness of the compressed surface and the alignment of the chain axis with the stress. The highest observed values of the ultimate strength are most indicative of the intrinsic strength of the material.

3.1.2. Stress perpendicular to b

Fig. 10 shows the stress–strain behaviour for the stress perpendicular to *b*. Again, the unloading–reloading behaviour was typically metallic. No maximum occurred in the stress–strain curve. The crystal flattened and fibrilated as shown in the photographs (Figs. 11). The splintered appearance of the crystals that were deformed with the stress parallel to *b* does not occur with the stress perpendicular to *b*. Even though the fibrilated crystal has a porous appearance, no volume change could be measured after deformation within the error of measurement of about 10%. It is to be noted that all the displacement (Figs. 11c and d) occurred transverse to the chain axis. The dimensions of the crystal in the *b* direction do not change as long as the stress is simple compression.

The true stress–strain curve of Fig. 10 is shown in Fig. 12. Work hardening of the crystal during fibrilation is indicated. If the fibrils become bent as the crystal is being flattened then some type of work hardening would be expected. Fig. 13 shows the structure of a flattened and fibrilated crystal where the bending and misalignment of the fibrils is more evident. This bending and misalignment would make crystal glide with more difficulty and produce work hardening.

Figure 13 Photograph of a deformed crystal showing a large crack-like shear displacements parallel to the *b*-axis.

Fig. 13 also shows fibrilation with the major component of displacement being perpendicular to *b*. There is also some displacement parallel to *b* which is no doubt caused by the stress field not being pure compression but having a component of shear stress parallel to *b*. The latter component of stress was introduced by the irregularity in the shape of the specimen.

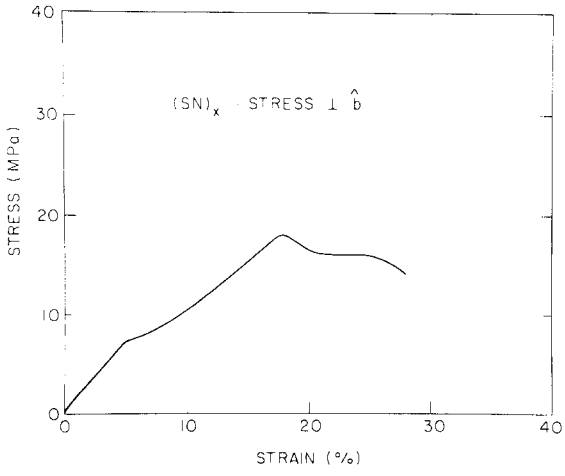

Figure 14 Stress–strain curve for crystal E.

Whereas some crystals with the stress perpendicular to b showed a uniform flattening and work hardening after yielding (Fig. 12), other crystals exhibited a maximum in the stress–strain curve as shown in Fig. 14. The collapsed crystal that produced Fig. 14 is shown in Fig. 15. This crystal shows gross deformation and fibrilation exhibited by the crystal in Fig. 11. Probably the difference between the collapse behaviour in Fig. 14 and the yield and work hardening behaviour of Fig. 10 should be attributed to their having different orientations. The latter behaviour is expected if crystal slip occurs.

Yielding or collapse occurred at stresses ranging from 14 to 24 MPa. These values are significantly below the strength (15 to 74 MPa) with the stress parallel to b. The highest values of the strength that have been observed are the most significant indicators of the intrinsic strength of the material, whereas the low values reflect the irregularities in the shape of the crystals. These irregularities produce stress concentrations which cause the crystal to yield or collapse under a low load.

3.2. Elastic moduli

From the slopes of the stress–strain curves during elastic unloading and reloading, Young's modulus was calculated. The maximum displacement during the elastic deformation was on the limit of the experimental uncertainty in the strain measurement. It was found that $E_{\parallel} = 21$ GPa ± 50% and $E_{\perp} = 1.4$ GPa ± 50%. These values are considered to be significant because they agree favourably with the values obtained from the velocity of sound measurements [15] where $E_{\parallel} = 29.8$ GPa and $E_{\perp}(\text{av}) = 4.8$ GPa.

4. Discussion

The key to understanding the stress–strain behaviour of the single crystal is by determining the likely slip systems. This determination is based on (1) the modes of deformation as exhibited by Figs. 9b, 11d, 13, and 15, (2) the types of bonding in the crystal, and (3) the steric hindrance which results during the operation of a slip system. Knowing the probable slip system and the stress–strain behaviour of the imperfectly shaped crystals, it

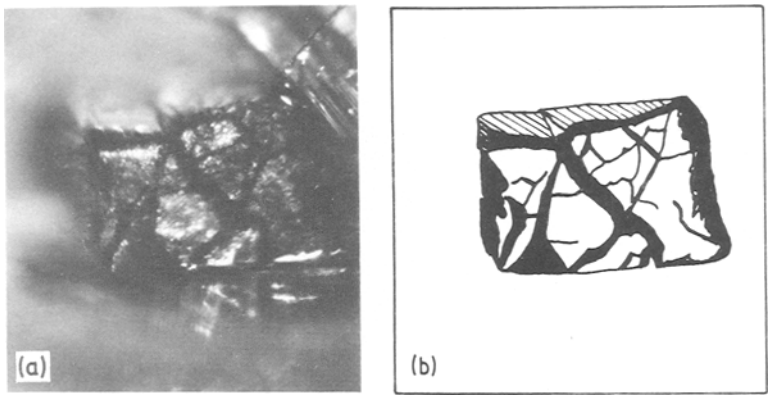

Figure 15 Deformed crystal E.

was of interest to speculate on the types of stress–strain behaviour that should be expected from a uniaxial stress on crystals of the ideal shape.

4.1. The slip mechanism

4.1.1. The easy slip system; (1 0 0), [0 0 1]

Slip is expected on that slip plane and direction which allows the atoms to pass one another with a minimum steric hindrance and does not require strong (covalent type) bonds to be broken. Slip only on $\{h\,0\,l\}$ planes is expected because these would not cut the strong bonds along the chain. Of the $\{h\,0\,l\}$ planes the ones with the greatest interplanar spacing are the most likely glide planes; these are the (1 0 0), (0 0 2) and (1 0 $\bar{2}$) whose interplanar spacings are 3.966, 3.607, and 3.245 Å respectively. In addition various glide directions in these planes were analysed with respect to the maximum steric hindrance that would occur during glide. This analysis was based on the hard sphere model which is an excellent model for van der Waals bonds. It was found that (1 0 0) slip in the [0 0 1] direction produced only a very slight change in the sulphur–sulphur (S–S) bond distance. An analysis of the ($\bar{1}$ 0 2) slip planes, which is the plane of the chain, showed that the [2 0 1] and [0 1 0] directions required about a 10 to 12% decrease in the S–S bond distance. Slip on the (0 0 1)[1 0 0] system required a 25% decrease in the S–N bond distance. Since the maximum interplanar spacing occurs on the (1 0 0) and the minimum steric hindrance occurs during slip of the (1 0 0), [0 0 1] system it is concluded that the (1 0 0), [0 0 1] system is the one of easiest glide.

Baughman *et al.* [12–14] have also come to this conclusion, which was supported by their observation of a shear-induced phase transformation by a (1 0 0), $\frac{1}{2}$ [0 0 1] shear.

4.1.2. Dislocation behaviour on the (1 0 0), [0 0 1] slip system

There is expected to be an appreciable difference between the mobility of edge and screw dislocations on the (1 0 0), [0 0 1] system. The motion of the edge dislocations involves a rotation of the chains around the [0 1 0] axis whereas screw motion requires a bending of the chains out of their plane. The latter motion involves the bending of highly directional intra-chain bonds.

Baughman *et al.* [12–14] observed that $(SN)_x$ crystals partially transform from the monoclinic to orthorhombic structure when deformed by grinding or by compression, as in Fig. 13. They showed that the phase transformation most likely occurred by a (1 0 0), $\frac{1}{2}$ [0 0 1] shear. This result indicates that the extended unit [0 0 1] dislocation with partial $\frac{1}{2}$ [0 0 1] dislocations is likely to occur. Stacking faults from $\frac{1}{2}$ [0 0 1] slip should also exist in the deformed crystal.

4.1.3. The effect of twin boundaries on deformation

(1 0 0) planes may also be the boundary plane between the twin domains (Fig. 3) which were produced by the two possible modes of polymerization. Whether slip is more likely to take place on a plane between the twins rather than within the twin is an open question. However, fracture would probably take place more readily at the twin boundary and thus produce the fibrilated structure that is observed (Figs. 3, 9b, 11d, and 13).

4.2. Types of stress–strain curves

We will speculate on the types of stress–strain curves that would be expected for crystals of the ideal shape for a uniaxial compressive stress and with the stress either parallel or perpendicular to b (chain axis).

4.2.1. Stress parallel to b

In this direction no slip is expected because strong covalent bonds would have to be broken. The crystal should load elastically until the crystal collapses by the splintering and fragmentation process exhibited in Fig. 9b. The maximum stress should depend critically on the perfection of the alignment of the chain axis relative to the stress. The maximum stress would also depend on the ratio of the height to the width of the crystal, as for the buckling of an elastic column. Under the most favourable conditions the collapse stress will be less than the theoretical strength, which is about $E_{\parallel}/10 = 2000$ MPa. A probable intrinsic stress–strain curve is depicted in Fig. 16a.

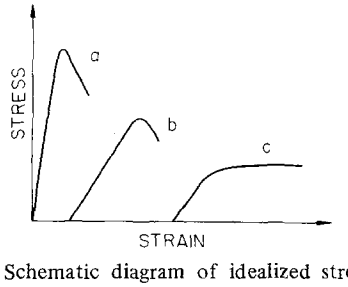

Figure 16 Schematic diagram of idealized stress–strain curves for $(SN)_x$ single crystals.

4.2.2. Stress perpendicular to b

If the crystal is oriented so that the (1 0 0) plane is perpendicular to the compressive stress or the [0 0 1] is parallel to it, then the resolved shear stress on the (1 0 0), [0 0 1] slip system is zero. Fracture rather than glide becomes more likely and the collapse type of stress–strain behaviour indicated in Fig. 16b is expected. The stress–strain behaviour would be similar to Fig. 16a except that the elastic modulus is lower and the collapse load would be less. The collapsed state would be like Fig. 15 instead of Fig. 9b.

If the crystal is oriented so that the (1 0 0), [0 0 1] can operate, then yielding and work hardening is expected (Fig. 16c) in accordance with behaviour observed in Figs. 10 and 12. Our limited experimental observation indicates that the critical shear stress for yielding is probably less than 5 MPa. The work hardening that occurs is probably caused by the bending and misalignment of the chains during the slip process, as indicated by the fibrilated structure shown in Figs. 11d and 13.

4.3. Comparison of mechanical properties of $(SN)_x$ with other materials

4.3.1. Loading–reloading behaviour

All the stress–strain curves showed that $(SN)_x$ unloads and reloads according to linear elastic behaviour with the yield point on reloading being about the same as the stress prior to unloading. This behaviour is typical of a highly crystalline solid. An amorphous or semi-crystalline polymer, on the other hand, shows a large hysteresis loop and non-linear behaviour during unloading and loading, and the strain recovered during unloading is about 4 to 8%, which is about the same as the strain at yielding.

4.3.2. Ultimate strength and yield point

The yield stress in shear of $(SN)_x$ is less than about 5 MPa which is about the value of 4 MPa for pure copper [16] crystals. The compressive strength of $(SN)_x$ ranged from 24 to 74 MPa with the stress perpendicular to and parallel to the chains, respectively. This strength would no doubt be greater if the crystals had the ideal shape. For comparison, a linear unoriented polymer has yield points that range from 14 to 80 MPa at room temperature [17].

Chiang *et al.* [18] showed that for tension parallel to the chain axis, $(SN)_x$ could sustain a stress of at least 300 MPa. This may be compared with oriented polymer fibres such as cellulose acetate, polyethylene and nylon whose average tensile strengths are 168, 480 and 640 MPa [17], respectively.

4.3.3. Young's modulus, E

Our values of $E_{\parallel} = 21$ GPa and $E_{\perp}$ 1.4 GPa compare favourably with the values of $E_{\parallel} = 30$ GPa and $E_{\perp}(\text{av}) = 5$ GPa from the velocity of sound measurements [15]. For comparison, E of polycrystalline copper is 111 GPa [17] and for unoriented polymethylmethacrylate at room temperature $E = 2.4$ GPa [19].

If one wants to compare the mechanical properties on the basis of density then it should be noted that the densities of copper, PMMA polymer and $(SN)_x$ are 8.9, 1, and 2.31 g cm^{-3} respectively [8].

The elastic anisotropy factor, $E_{\parallel}/E_{\perp}$ is about 15. This value is about the same as the anisotropy factor for the intrinsic electrical conductivity and the optical reflectance [3–9]. For polyethylene and polyvinyl chloride $E_{\parallel}/E_{\perp} = 75$ and 29 respectively [20]. These results indicate that $(SN)_x$ is more like an anisotropic metal than a single crystal of an ordinary polymer.

In order to explore more detailed mechanical properties of this novel metallic polymer $(SN)_x$, measurements performed on completely oriented single crystal are preferred. Also tensile and shear measurements should yield more information in future studies.

5. Conclusion

We have studied the mechanical properties of single crystal $(SN)_x$. The stress–strain curves are measured in directions parallel and perpendicular to the chain axis. The stress–strain behaviour of $(SN)_x$ most resembles that of a highly anisotropic metal. The unloading–reloading behaviour from the plastic state of $(SN)_x$ is metal-like. The elastic anisotropic factor determined from this measurement is about 15. This anisotropic factor agrees with those obtained from the studies of electronic properties.

$(SN)_x$ probably has a single easy glide system which is most likely (1 0 0)[0 0 1]. The chain structure of the atoms causes the fibrilated morphology of the deformed state.

Acknowledgements

We are grateful to Professor A. G. MacDiarmid for his encouragement which got us started in this research and for supplying us with the crystals of $(SN)_x$. One of us (CKC) wishes to acknowledge with gratitude the support of Professors A. J. Heeger and A. F. Garito during various stages of this work.

References

1. V. V. WALATKA Jr, M. M. LABES and J. H. PERTSTEIN, *Phys. Rev. Lett.* **31** (1973) 1139.
2. C. HSU and M. M. LABES, *J. Chem. Phys.* **61** (1974) 4640.
3. A. A. BRIGHT, M. J. COHEN, A. F. GARITO, A. J. HEEGER, C. M. MIKULSKI, P. J. RUSSO and A. G. MacDIARMID, *Phys. Rev. Lett.* **34** (1975) 206.
4. A. A. BRIGHT, M. J. COHEN, A. F. GARITO, A. J. HEEGER, C. M. MIKULSKI and A. G. MacDIARMID, *Appl. Phys. Lett.* **26** (1975) 612.
5. R. L. GREENE, P. M. GRANT and G. B. STREET, *Phys. Rev. Lett.* **34** (1975) 89.
6. R. L. GREENE, G. B. STREET and L. J. SUTER, *ibid.* **34** (1975) 557.
7. C. K. CHIANG, M. J. COHEN, A. F. GARITO, A. J. HEEGER, C. M. MIKULSKI and A. G. MacDIARMID, *Solid State Comm.* **18** (1976) 1451.
8. C. M. MIKULSKI, P. J. RUSSO, M. S. SARAN, A. G. MacDIARMID, A. F. GARITO and A. J. HEEGER, *J. Amer. Chem. Soc.* **97** (1975) 6358.
9. M. J. COHEN, A. F. GARITO, A. J. HEEGER, A. G. MacDIARMID, C. M. MIKULSKI, M. S. MORAN and J. KLEPPINGER, *ibid.* **98** (1976) 3844.
10. A. BONDI, "Physical Properties of Molecular Crystals, Liquids and Glasses" (John Wiley, New York, 1968).
11. R. H. BAUGHMAN, R. R. CHANCE and M. J. COHEN, *J. Chem. Phys.* **64** (1976) 1869.
12. R. H. BAUGHMAN, P. A. APGAR, R. R. CHANCE, A. G. MacDIARMID and A. F. GARITO, *J. C. S. Chem. Comm.* (1977) 49.
13. R. J. YOUNG and R. H. BAUGHMAN *J. Mater. Sci.* **13** (1978) 55.
14. R. H. BAUGHMAN, P. A. APGAR, R. R. CHANCE, A. G. MacDIARMID and A. F. GARITO, *J. Chem. Phys.* **66** (1977) 401.
15. H. J. STOLZ, H. WENDEL, A. OTTO, L. PINTSCHOVIUS and H. KAHLERT, *Phys. Stat. Sol.* **78** (1976) 277.
16. G. ARDLEY and A. H. COTTRELL, *Proc. Roy. Soc.* **A219** (1953) 328.
17. "Materials Engineering", Materials Selector Issue (Rheinhold, New York, 1968).
18. C. J. CHIANG, A. J. HEEGER and A. G. MacDIARMID, *Phys. Lett.* **60A** (1977) 375.
417.
20. I. SAKURADA, T. ITO and K. NAKAMAE, *J. Polymer Sci., Part C* **15** (1966) 75.

Received 8 March and accepted 15 May 1978.